Preprints (www.preprints.org) | NOT PEER-REVIEWED | Posted: 17 April 2023 doi:10.20944/preprints202304.0412.v1

Disclaimer/Publisher's Note: The statements, opinions, and data contained in all publications are solely those of the individual author(s) and contributor(s) and not of MDPI and/or the editor(s). MDPI and/or the editor(s) disclaim responsibility for any injury to people or property resulting from any ideas, methods, instructions, or products referred to in the content.

Article

Analysis of Flow Characteristics of a Debris Filter in a Condenser Tube Cleaning System

Da Woon Jung[1], Young-Chan Lim[1], Chung-Won Seo[1], Dong Sun Kim[2], Seung Yul Lee[2], and Hyun Kyu Suh*

[1] Graduate School of Mechanical Engineering, College of Engineering, Kongju National University, Chungnam 31080, Republic of Korea; dwjung@smail.kongju.ac.kr
[2] Jeong-woo Industrial Machine Co., Ltd, 253,5 Sandan-ro, Susin-myeon, Dongnam-gu, Cheonan-si, Chungnam 31251, Republic of Korea; leesy@jimc.co.kr ; dskim@jimc.co.kr
* Correspondence: hksuh@kongju.ac.kr; Tel.: +82-41-521-9264

Abstract: In a power plant that uses seawater as a coolant, the debris filter (DF) is required to remove foreign substances from the seawater, and differential pressure leads to a decrease in the coolant flow rate, leading to a decrease in power generation efficiency. In this study, analysis was performed under different initial flow velocity conditions of 1.5 m/s, 2.0 m/s, and 2.5 m/s for a DF used in a power plant to understand flow characteristics in condenser tube cleaning system (CTCS). The flow and differential pressure characteristics of a CTCS with an installed DF were considered in a comparative analysis of velocity, pressure, and turbulence kinetic energy (TKE) distributions. The results confirmed that a vortex was generated in the pipe with the DF, apparently due to the collision of the flow with the bracket of the DF. As the flow rate increased, the range of the vortex increased, causing a loss in flow.

Keywords: Condenser tube cleaning system (CTCS); Debris filter (DF); Differential pressure; Fluid resistance; Pressure drop; Turbulence kinetic energy (TKE); Flow vortex

1. Introduction

The reckless use of primary energy such as oil, coal, natural gas, and nuclear power due to advanced industrialization has led to the depletion of fossil fuels and environmental problems caused by global warming. As a result, the productivity and technological importance of the energy industry have become very important. In particular, for countries that need to import resources and convert them into secondary energy to produce electricity, efficient development based on economic stability is essential [1-3].

One of the most influential equipments in power plants, the condenser plays a role in increasing efficiency by rotating the turbine and generator with high-pressure and high-temperature steam and is very important for energy production because it reuses steam.

In the literature, studies have been conducted to improve the performance of capacitors by utilizing various parameters. Ibrahim et al. studied the effect of the fouling of condenser tubes on thermal performance in nuclear power plants and found that an increase in fouling factor causes a decrease in thermal efficiency and power loss [4]. Alabrudzinski et al. performed simulations based on computational fluid dynamics (CFD) analysis using the fouling thermal resistance value according to the fouling growth rate measurement results and turbine operating conditions. They found that the thermal resistance of fouling reduces the output of the turbine and that even an old condenser can affect the output of the turbine [5]. Pattanayak et al. analyzed various parameters that affect the efficiency of steam condensers through simulation models based on thermodynamic theory. They derived the cooling water temperature that can maintain the optimal condenser pressure and found that as the cooling water temperature increases, the heat rate of the power cycle decreases [6]. Mohammadaliha et al. developed a new air-to-liquid cross-flow

© 2023 by the author(s). Distributed under a Creative Commons CC BY license.

heat exchanger model to analyze the effect of thermal conductivity on overall efficiency in condenser heat exchangers. They found that materials with excellent corrosion resistance and low-cost materials have low thermal characteristics that affect performance and that if materials with a thermal conductivity value of less than 0.5 W/m·K are used, the efficiency of heat recovery systems is significantly reduced [7]. Gadhamshetty et al. used a new approach, a cooling water heat energy storage system, to improve the performance degradation due to ambient temperature rise, which is a disadvantage of air-cooled condensers (ACC) environmentally compared to water-cooled condensers in heat dissipation. They confirmed that power loss can be reduced through thermodynamic modeling and simulation [8].

Most power plants use seawater as a coolant, which introduces various impurities and foreign substances such as seaweed and fish eggs into the seawater. This provides an environment for microbial growth, and the impurities adhere to the surface of the condenser tube, reducing the heat exchange performance of the condenser and increasing the exhaust pressure of the steam turbine, which can cause safety issues and lead to a decrease in power generation efficiency and power production efficiency [9]. To solve this, as shown in Figure 1, the DF is installed in front of the condenser to filter the seawater. The DF is composed of screen, rotor, and hopper. It filters foreign substances contained in seawater using a screen and absorbs and removes the various foreign substances that accumulate using a rotor and hopper. However, in this process, foreign substances that are filtered by the screen and accumulate can create a differential pressure. This can decrease the flow rate of cooling water flowing into the condenser, which leads to a decrease in the heat exchange efficiency of the condenser and the stability of the circulating water pump [10,11].

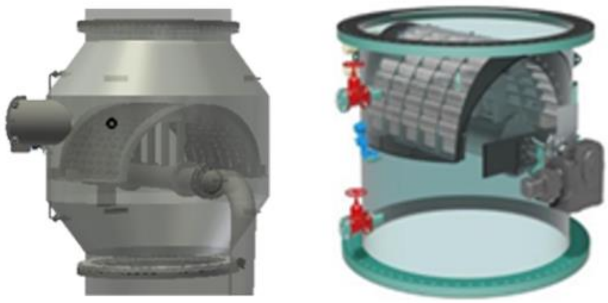

Figure 1. The shape and position of the DF inside the CTCS.

Until recently, research to improve condenser heat exchange performance has primarily focused on improving the recovery and circulation rate of sponge balls and reducing ball loss, by considering the flow characteristics of the CTCS in which the sponge balls are applied [12-14]. Jung et al. conducted the DF flow tests for two types of DF, P-grid and G-grid, using 18 types of debris. They found that the G-grid filter design showed better performance than the P-grid design because it provided a smaller flow area and higher grid strap than the P-grid design [15]. In addition, Walker et al. analyzed the economic impact of fouling on the condenser to analyze the cleaning system for economic cost analysis and found that increasing the cleaning frequency can reduce additional fuel costs due to fouling [16]. In another work, Chae et al. conducted an experimental study to maintain the efficiency of plate heat exchangers while eliminating the inconvenience of cleaning operations and measured the recovery rate according to changes in flow rate within the tube and changes in cleaning time and recovery time [1]. Kim et al. conducted an experiment-based study to solve the stability problem caused by excessive vibration during circulating water pump operation. They revealed how the operating characteristics of the DF affected the natural vibration of the pump, and suggested ways to reduce vibration [17].

Preprints (www.preprints.org) | NOT PEER-REVIEWED | Posted: 17 April 2023 doi:10.20944/preprints202304.0412.v1

In this study, research was conducted to improve the performance of the CTCS equipped with a DF that is currently installed in existing power plants. Due to the pressure drop caused by fluid pressure, which limits the stability of the fluid pump and the efficiency of heat exchange, numerical analysis was performed to analyze the flow characteristics inside the system's pipes and identify factors affecting pressure drop and fluid resistance. It was confirmed that the pressure drop caused by the screen that filters out the DF and external substances is a factor that affects it, and by analyzing the correlation between the shape of the screen that can minimize pressure drop and the size of the perforated plate, we derived an optimal screen shape according to DF size through CFD analysis. In addition, the effects of the presence or absence of the filter on flow characteristics and differential pressure performance in the pipe according to each initial flow rate condition were compared and analyzed, and the velocity, pressure, and TKE distribution in the pipe according to flow rate were examined for comparison and analysis.

2. Numerical analysis method

2.1. Numerical analysis target and design conditions

This study was conducted to investigate the effect of the presence or absence of the DF, and the flow velocity on the differential pressure and TKE. A numerical analysis modeling was performed using a 14-inch DF that was actually in use, as shown in Figure 2 (a). The height of the mid-plate and the size of the perforated plate for fixing the screen were set to 30 mm. Fluid analysis was conducted using commercial code and the fluid region of Figure 2(a) was extracted to create mesh for analysis. Water-liquid was applied as the working fluid. In addition, as shown in Figure 2 (b), to derive the results of velocity, pressure, and TKE, the vertical direction (H) was set at an interval of 0.06 m, and the horizontal direction (L) was set at 0.333 m intervals from the bottom of the inlet in the center plane of the pipe. Each of the points used for measuring flow characteristics is plotted in this figure and The conditions were set with the goal of establishing a numerical analytical database for the shape.

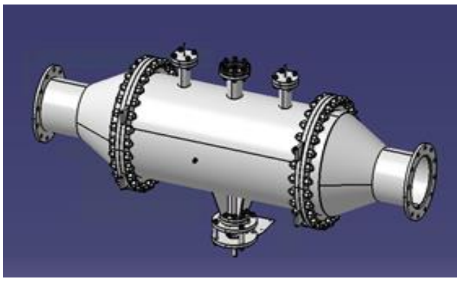

(**a**)

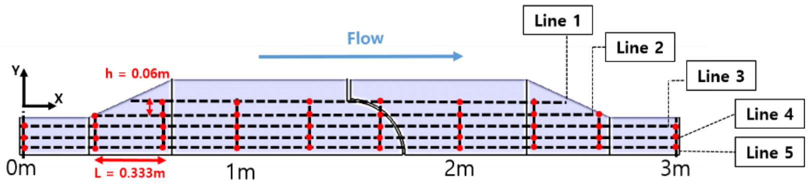

(**b**)

Figure 2. Schematics of the DF and flow characteristics measuring points: (**a**) Schematics of the DF and (**b**) Measuring points of pipe with the DF applied.

2.2. Governing Equations for Numerical Analysis

As the governing equations for flow analysis, continuity equations, momentum equations, and energy equations were applied, and they are expressed as the following equations.

$$\frac{\partial u}{\partial x} + \frac{\partial v}{\partial y} + \frac{\partial w}{\partial z} = 0 \tag{1}$$

$$u\frac{\partial u}{\partial x} + v\frac{\partial v}{\partial y} + w\frac{\partial w}{\partial z} = -\frac{\partial p}{\partial x}\frac{1}{\rho} + \nu_e\left(\frac{\partial^2 u}{\partial x^2} + \frac{\partial^2 u}{\partial y^2} + \frac{\partial^2 u}{\partial z^2}\right) \tag{2}$$

Preprints (www.preprints.org) | NOT PEER-REVIEWED | Posted: 17 April 2023 doi:10.20944/preprints202304.0412.v1

$$u\frac{\partial u}{\partial x}+v\frac{\partial v}{\partial y}+w\frac{\partial w}{\partial z}=-\frac{\partial p}{\partial x}\frac{1}{\rho}+\nu_e(\frac{\partial^2 v}{\partial x^2}+\frac{\partial^2 v}{\partial y^2}+\frac{\partial^2 v}{\partial z^2})$$

$$u\frac{\partial u}{\partial x}+v\frac{\partial v}{\partial y}+w\frac{\partial w}{\partial z}=-\frac{\partial p}{\partial x}\frac{1}{\rho}+\nu_e(\frac{\partial^2 w}{\partial x^2}+\frac{\partial^2 w}{\partial y^2}+\frac{\partial^2 w}{\partial z^2})$$

$$u\frac{\partial T}{\partial x}+v\frac{\partial T}{\partial y}+w\frac{\partial T}{\partial z}=\alpha(\frac{\partial^2 T}{\partial x^2}+\frac{\partial^2 T}{\partial y^2}+\frac{\partial^2 T}{\partial z^2}) \quad (3)$$

In equations (1) to (3), u, v, and w represent the speed in the x, y, and z directions, respectively, ρ is the density, and v is the coefficient of kinematic viscosity. For the turbulence model, the shear-stress transport (SST) model suitable for the $k-\omega$ model-based flow separation simulation is applied, and the flow field is calculated based on the TKE (k) and energy-specific dissipation rate (ω) equations.

$$\frac{\partial}{\partial t}(\rho k)+\frac{\partial}{\partial x_i}(\rho k u_i)=\frac{\partial}{\partial x_j}\left[\Gamma_k\frac{\partial k}{\partial x_j}\right]+G_k+G_b-Y_k+S_k \quad (4)$$

$$\frac{\partial}{\partial t}(\rho\omega)+\frac{\partial}{\partial x_i}(\rho\omega u_i)=\frac{\partial}{\partial x_j}\left[\Gamma_\omega\frac{\partial k}{\partial x_j}\right]+G_\omega+G_{\omega b}-Y_\omega+S_\omega \quad (5)$$

G_k represents the generation of the TKE due to the velocity gradient, and G_ω is the energy-specific dissipation rate (ω) generation term. Γ_k, and Γ_ω mean the effective diffusion of k and ω due to turbulence, Y_k, and Y_ω are the dissipation terms of k and ω due to turbulence, S_k, and S_ω are user-defined terms, and the Eddy viscosity in the $k-\omega$ turbulence model $\mu_t=\rho k/\omega$ is calculated.

2.3. Verification of Numerical Analysis Results

Before numerical analysis, about 1.3 million tetra meshes were generated by extracting the fluid area in the pipe to which a 14-inch DF was applied. Detailed information about the mesh applied to the numerical analysis is shown in Table 1 and Figure 3. Based on the differential pressure results for each flow velocity obtained in the experiment, the differential pressure displayed by the screen (perforated plate) in the DF was simulated to be the viscous resistance value of a porous zone, similar to the experimental value. The normalized differential pressure results are shown in Figure 4. After normalization, it was confirmed that at the highest initial flow velocity of 2.5 m/s, the maximum error was 6.99%, and the experimental values and the trend of numerical analysis were the same in all flow rate conditions. Accordingly, it was judged that the reliability of this study was secure.

Table 1. The amount of mesh used for the numerical analysis.

Cases	Nodes	Elements
With DF	260,950	1,308,948
Without DF	51,297	259,098

Preprints (www.preprints.org) | NOT PEER-REVIEWED | Posted: 17 April 2023 doi:10.20944/preprints202304.0412.v1

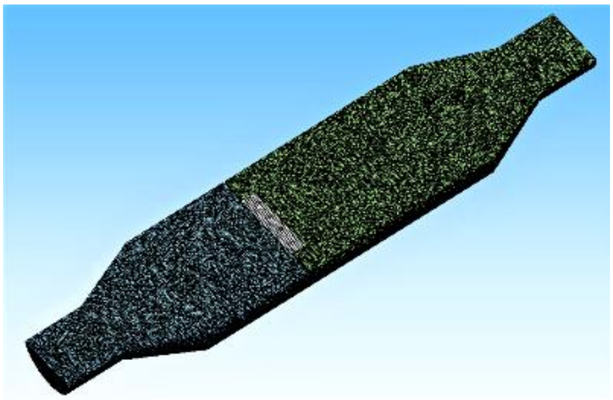

Figure 3. Mesh of pipe with the DF applied.

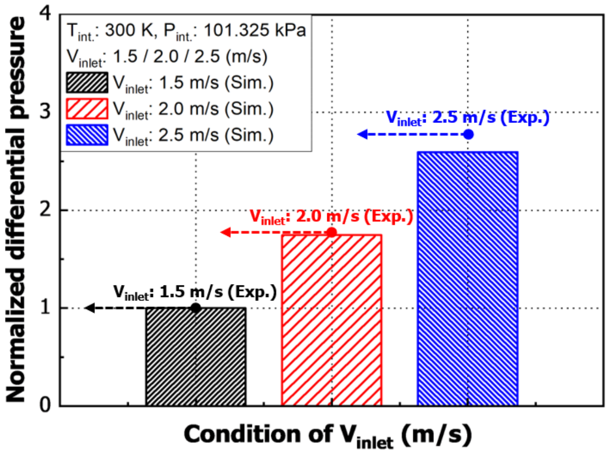

Figure 4. Normalized results for differential pressure under various flow velocity.

2.4. Numerical Analysis Conditions

Steady-state analysis was carried out by applying the analysis conditions shown in Table 2, based on the grid used to verify the analysis results. To analyze the TKE and differential pressure characteristics in the presence or absence of the DF, a numerical analysis was performed on the pipe of the CTCS with or without 14-inch DF cases. The working fluid was set as water-liquid, and the flow rates were 1.5 m/s, 2.0 m/s, and 2.5 m/s. Then the flow characteristics in the CTCS were compared and analyzed according to the flow rates.

Table 2. Numerical Analysis conditions.

Contents	Conditions
Turbulence model	$k-\omega$ (sst)
Inlet velocity (m/s)	1.5, 2.0, 2.5
Inlet temperature (K)	300
Inlet pressure (kPa)	101.325
Outlet condition	Pressure outlet

3. Numerical analysis results

3.1. Effect of the DF on flow rate

Figure 5 shows the velocity distributions in the pipe with and without the DF applied, and Table 3 shows the velocity values in the pipe according to the inlet flow rate change. In the velocity distribution when the DF was on the left side of Figure 5, the main flow at the front end before passing the filter was distributed in the center of the pipe. In

Table 3, the porous zone is located at point 6, and it can be seen that the velocity results are generally higher at points 3, 4, and 5. Without the DF on the right side of Figure 5, the main flow was distributed near the wall of the pipe. As seen through streamline in Figure 5, This suggests that the main flow forms in the center of the tube because a vortex is generated by the flow colliding with the bracket at the top of the DF.

Table 4 shows the TKE values in the pipe according to the inlet flow rate change, and Figures 6 and 7 show the distribution of TKE and velocity in the tube of the CTCS with the DF. As shown in Figure 6, the TKE rapidly increases at the front end of the filter set as the porous zone. This suggests the main flow increases the resistance of the working fluid due to the viscous resistance of the porous zone. As the vortex generated by the flow colliding with the bracket at the top of the filter grows, it increasingly interferes with the main flow.

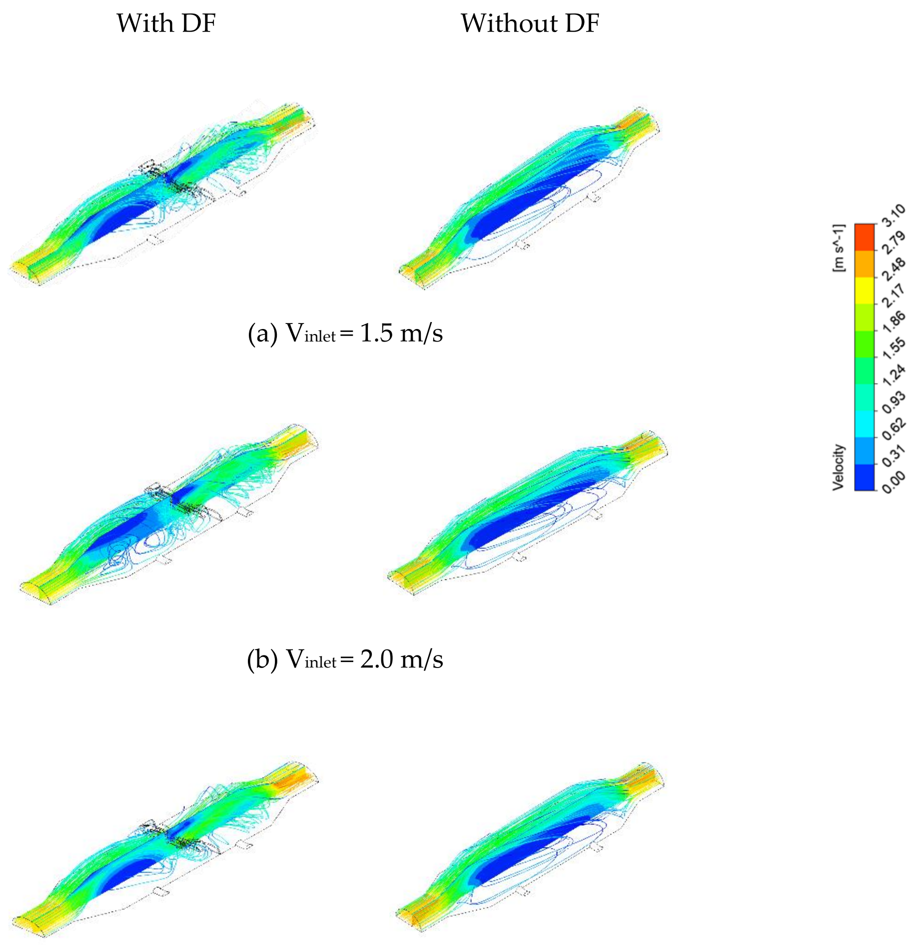

Figure 5. Comparison results of velocity contour with the DF (left) and without the DF (right) (a) V_{inlet} = 1.5 m/s, (b) V_{inlet} = 2.0 m/s, (c) V_{inlet} = 2.5 m/s.

Preprints (www.preprints.org) | NOT PEER-REVIEWED | Posted: 17 April 2023 doi:10.20944/preprints202304.0412.v1

Table 3. The velocity values at each flow characteristic measurement point in pipe containing DF.

V (m/s)											
V_{inlet}		Point 1	Point 2	Point 3	Point 4	Point 5	Point 6	Point 7	Point 8	Point 9	Point 10
1.5 m/s	Line 1			0.2297	0.1342	0.0325	0.4192	0.7169	0.8914		
	Line 2		0.1642	0.4782	0.377	0.28	0.1372	0.363	0.5899	1.5453	
	Line 3	1.5022	1.4826	1.4262	1.1571	0.8698	0.383	0.2178	0.3056	1.4089	1.5891
	Line 4	1.501	1.4862	1.4572	1.4166	1.3307	0.1246	0.1975	0.341	1.1407	1.4644
	Line 5	1.4991	1.4242	1.2668	1.2455	1.0776	0.3335	0.166	0.2726	0.9912	1.3142
2 m/s	Line 1			0.401	0.1639	0.1855	0.5385	0.915	1.1635		
	Line 2		0.3899	0.3994	0.4514	0.6452	0.189	0.4421	0.742	2.0443	
	Line 3	2.0024	1.9608	1.8216	1.4078	1.3166	0.53	0.3073	0.4525	1.8828	2.1836
	Line 4	2.0008	1.9639	1.9087	1.8297	1.6968	0.1748	0.2763	0.4724	1.5188	1.9404
	Line 5	2.0006	1.9615	1.906	1.8258	1.695	0.7811	0.2602	0.4588	1.4404	1.9276
2.5 m/s	Line 1			0.23	0.221	0.633	0.675	1.08	1.39		
	Line 2		0.195	1.02	1.14	1.34	0.242	0.54	0.839	2.5	
	Line 3	2.5	2.48	2.32	2.21	2.05	0.679	0.399	0.567	2.32	2.71
	Line 4	2.5	2.45	2.33	2.24	2.09	0.225	0.359	0.598	1.9	2.43
	Line 5	2.5	2.44	2.33	2.24	2.1	0.966	0.335	0.582	1.8	2.41

Table 4. The TKE values at each flow characteristic measurement point in pipe containing the DF.

TKE (m^2/s^2)											
V_{inlet}		Point 1	Point 2	Point 3	Point 4	Point 5	Point 6	Point 7	Point 8	Point 9	Point 10
1.5 m/s	Line 1			0.0382	0.0676	0.0539	0.0447	0.0347	0.0194		
	Line 2		0.0248	0.1010	0.1190	0.0938	0.0322	0.014	0.0263	0.0062	
	Line 3	0.0030	0.0004	0.0073	0.0577	0.0856	0.0181	0.0005	0.0032	0.0260	0.0260
	Line 4	0.0029	0.0004	0.0002	0.0001	0.0033	0.0030	0.0006	0.0022	0.0134	0.0135
	Line 5	0.0043	0.0054	0.0065	0.0070	0.0069	0.0107	0.0004	0.0011	0.0079	0.0107
2 m/s	Line 1			0.0580	0.1196	0.1157	0.0373	0.0436	0.0295		
	Line 2		0.0235	0.1925	0.2031	0.1504	0.0267	0.0160	0.0391	0.0097	
	Line 3	0.0043	0.0005	0.0332	0.1179	0.0780	0.0127	0.0088	0.0131	0.0410	0.0372
	Line 4	0.0042	0.0005	0.0002	0.0002	0.0005	0.0105	0.0080	0.0122	0.0363	0.0455
	Line 5	0.0041	0.0005	0.0002	0.0002	0.0001	0.0113	0.0051	0.0177	0.0650	0.0779
2.5 m/s	Line 1			0.0724	0.1796	0.1758	0.0558	0.0635	0.0467		
	Line 2		0.0729	0.2367	0.2678	0.1616	0.0408	0.0284	0.0506	0.0141	
	Line 3	0.0057	0.0006	0.0024	0.0082	0.0086	0.0516	0.0240	0.0180	0.0595	0.0539
	Line 4	0.0056	0.0006	0.0003	0.0002	0.0125	0.0968	0.0212	0.0185	0.0533	0.0711
	Line 5	0.0054	0.0006	0.0003	0.0002	0.0064	0.1417	0.0145	0.0256	0.1029	0.1283

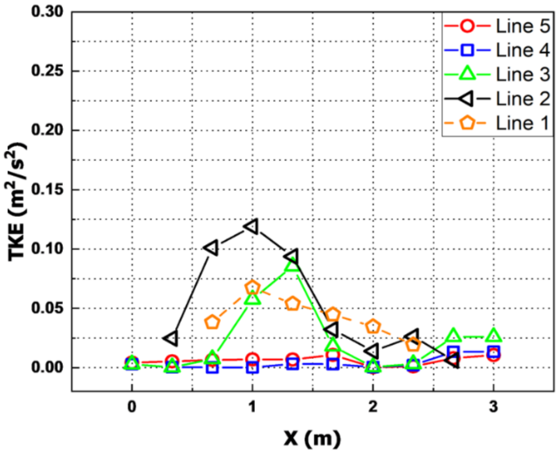

(a) V_{inlet} = 1.5 m/s

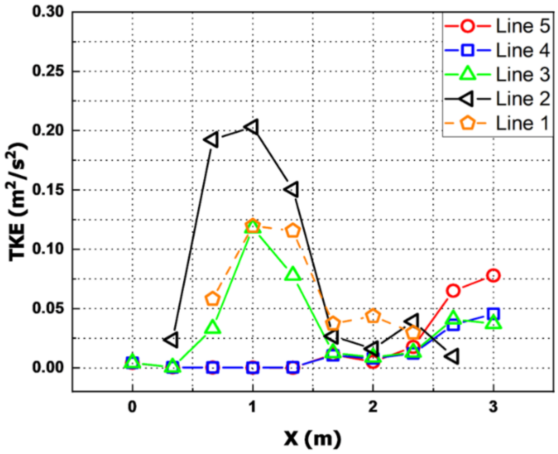

(b) V_{inlet} = 2.0 m/s

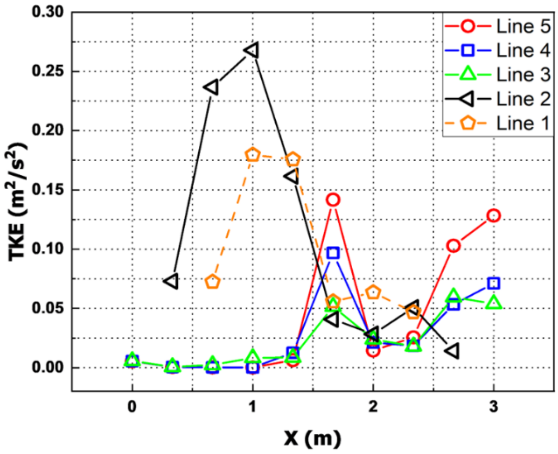

(c) V_{inlet} = 2.5 m/s

Figure 6. The TKE distributions of pipe with DF applied (a) V_{inlet} = 1.5 m/s, (b) V_{inlet} = 2.0 m/s, (c) V_{inlet} = 2.5 m/s.

 doi:10.20944/preprints202304.0412.v1

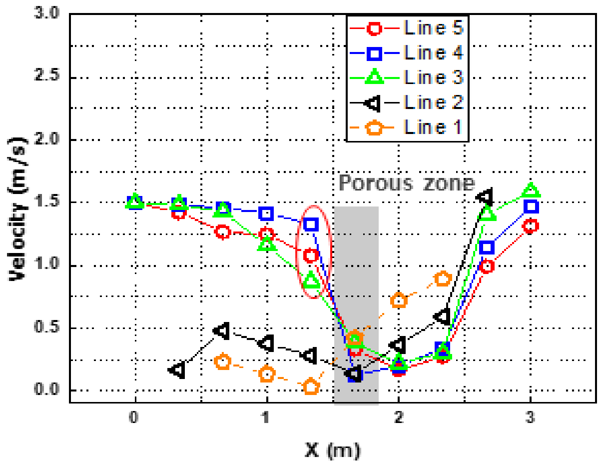

(a) V_{inlet} = 1.5 m/s

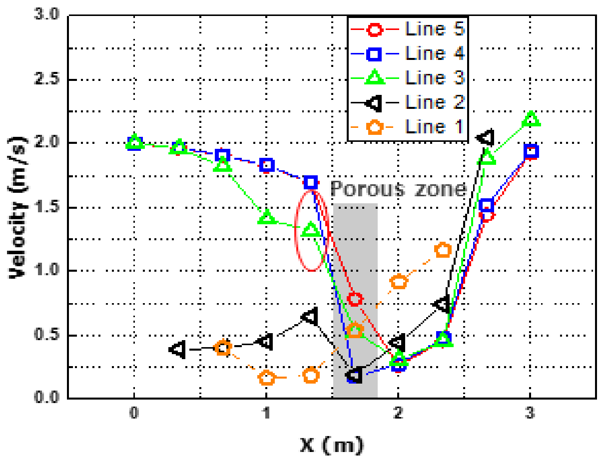

(b) V_{inlet} = 2.0 m/s

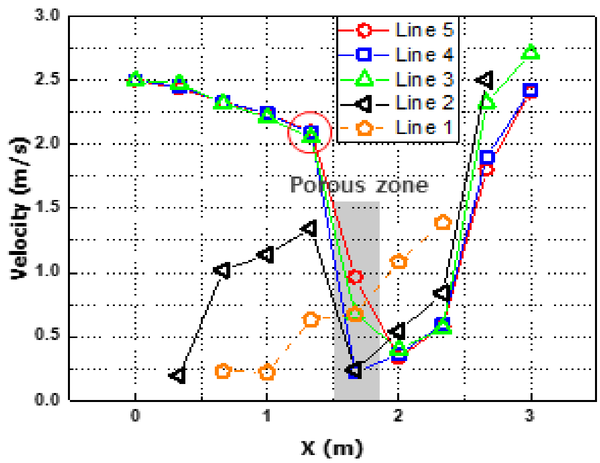

(c) V_{inlet} = 2.5 m/s

Figure 7. The velocity distributions of pipe with the DF applied. (a) V_{inlet} = 1.5 m/s, (b) V_{inlet} = 2.0 m/s, (c) V_{inlet} = 2.5 m/s.

Also, in the 2.5 m section in Figure 6, the TKE in Lines 3, 4, and 5 shows a tendency to increase again. This is because, as shown in the velocity distribution in the 2 m to 2.5 m section in Figure 7, the velocity of the main flow distributed along the wall of the tube increases due to the shape of the nozzle-shaped tube. The TKE increases as it affects the main flow due to the interaction with the relatively slower flow distributed in the center of the tube. The analyses confirmed that when the DF is applied, the main flow at the rear end is distributed along the wall of the tube, in contrast to the front end. This is because the bracket located on the top of the filter acts as a barrier, and the pressure at the rear end of the bracket is relatively lower than the pressure immediately after the porous zone. The working fluid that has passed through the filter tends to accelerate to the top of the filter with low pressure. This is judged to be the same as the tendency that the flow velocity of Line 1, the outer tube of the pipe at the point 2 m past the porous zone, appears higher than other points under all flow velocity conditions in Figure Line 3 in Figure 6 (c) under the 2.5 m/s flow rate, unlike (a) and (b), is similar to the trend of Lines 4 and 5 at the front of the porous zone. This indicates that as the flow rate increases, the range of the main flow increases so the trend of Line 3 became similar to the flow at the center of the pipe.

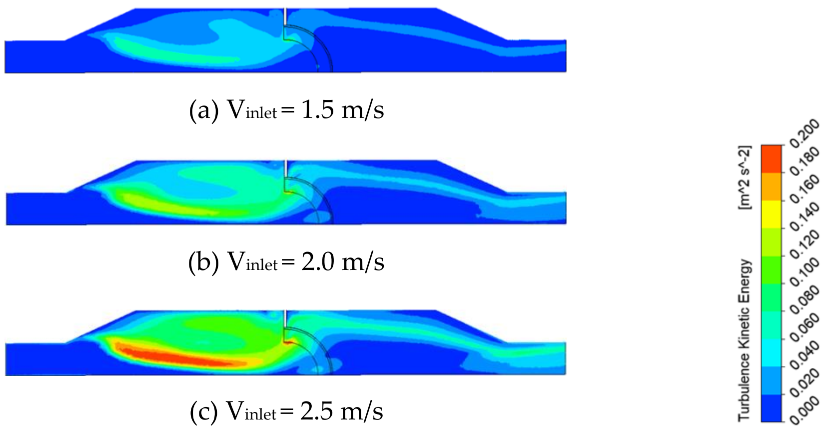

Figure 8. The TKE contour in a pipe with the DF. (a) V_{inlet} = 1.5 m/s, (b) V_{inlet} = 2.0 m/s, (c) V_{inlet} = 2.5 m/s.

Figure 8 shows the distributions of TKE concerning the flow velocity in the pipe with the DF applied. As the flow velocity increases, the effect of the area and value of the TKE at the front of the filter on the main flow increases, and it can be inferred that the distributions of the vortex increase. As the flow velocity increases, the radius of the vortex resulting from the flow colliding with the bracket at the top of the filter increases, and the friction with the main flow increases, showing the trend in Figure 8(c).

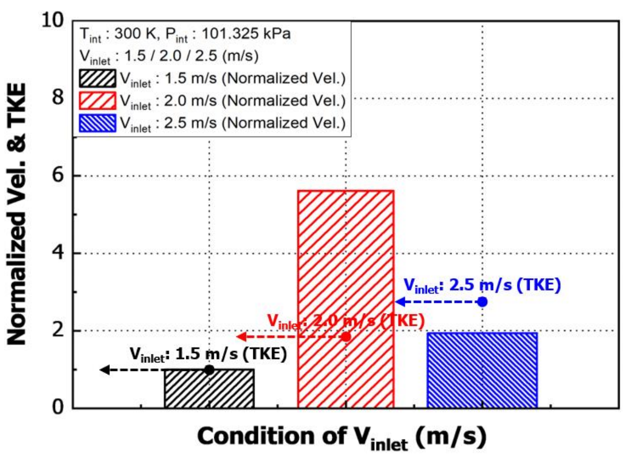

Figure 9. Normalized results for velocity and TKE under various flow velocity.

Figure 9 shows the normalized velocity and TKE under inlet flow conditions. The turbulence intensity generated by the working fluid is similar to the trend of the internal pressure distribution. In areas with high fluid resistance, fluid drag increases and flow separation occurs during fluid flow. As a result, it is judged that the flow characteristics deteriorated and the turbulence intensity increases due to the increase in pressure.

3.2. Pressure characteristics of the DF

Figure 10 indicates the pressure distributions for each flow velocity in the pipe with the DF, and the pipe without the DF, and Figure 11 presents the pressure variation in the pipe with the DF applied according to the measuring lines. Table 5 shows the pressure values in the pipe according to the inlet flow rate change. Figure 10 shows that the pressure at the front of the filter tends to increase rapidly as the flow rate increases. This indicates that an increase in flow velocity leads to an increase in the flow mass rate, and the pressure rises because the flow mass rate increases in the same volume. Thus, it was confirmed that the differential pressure was also increased by the filter, which could lead to the deterioration of the performance of the condenser.

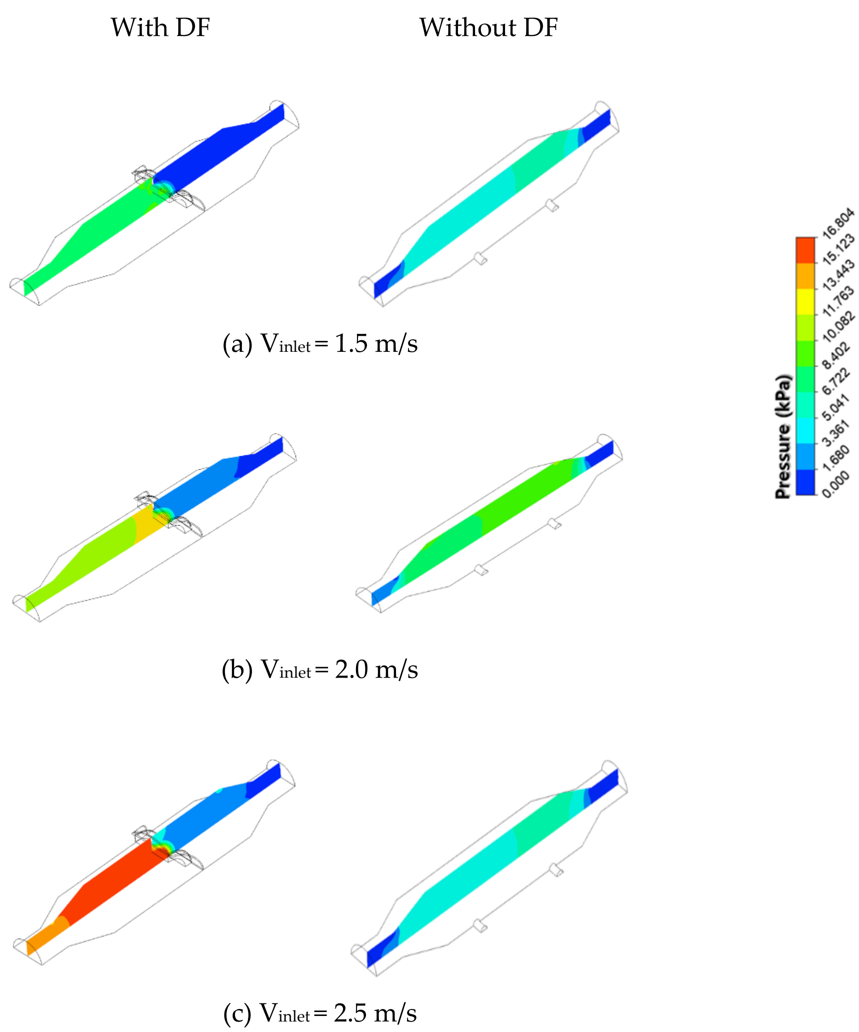

Figure 10. Comparison results of pressure contour with the DF (left) and without the DF (right) (a) V_{inlet} = 1.5 m/s, (b) V_{inlet} = 2.0 m/s, (c) V_{inlet} = 2.5 m/s.

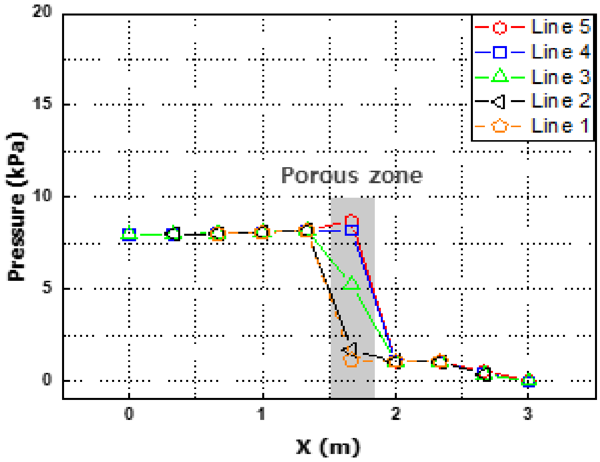

(a) V_{inlet} = 1.5 m/s

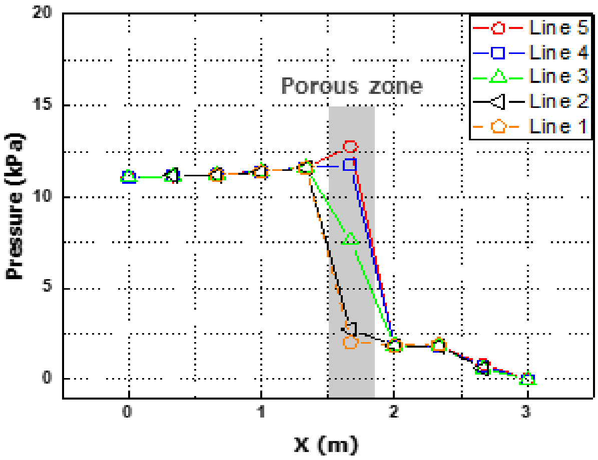

(b) V_{inlet} = 2.0 m/s

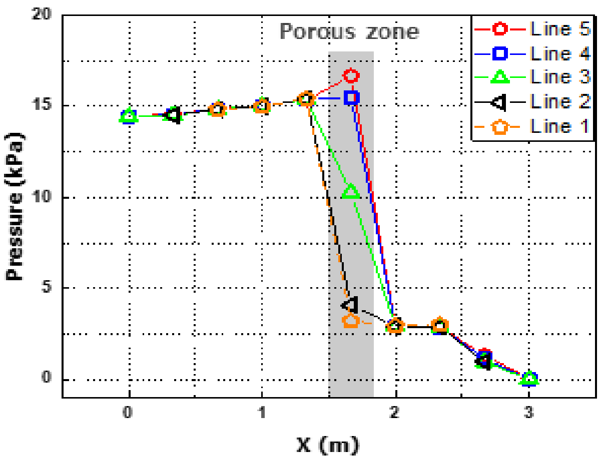

(c) V_{inlet} = 2.5 m/s

Figure 11. Pressure distributions of pipe with the DF applied. (a) V_{inlet} = 1.5 m/s, (b) V_{inlet} = 2.0 m/s, (c) V_{inlet} = 2.5 m/s.

In the pressure distribution in the pipe without the DF in Figure 10, both the inlet and outlet pressures were low, according to the Bernoulli's law, and the pressure tended to increase in the part of the expanded pipe where the flow rate was relatively low. On the other hand, in the pipe with the DF, the pressure at the front of the filter increased significantly compared to the case without the DF. It is believed that the pressure inside the pipe is increased significantly by the shape of the filter, the resistance generated by the bracket, and the influence of the pressure drop in the porous zone. It was also determined that the perforated plate of the filter and the shape of the filter have a dominant influence on the differential pressure performance. Thus, further research on this is necessary.

In Figures 7 and 11, as the flow rate increases, the velocity and pressure at the front end of the filter tend to increase. This is because the density per unit area at the outlet point of the pipe increases as the flow rate increases, which increases the kinetic energy of the fluid per the same unit area, meaning pressure will be high. At the same initial flow rate condition, the speed and pressure before and after the filter tend to be in inverse proportion, and the increase/decrease width for this tends to be large as the flow velocity increases. On the other hand, the velocity and pressure immediately after passing through the porous zone and filter tend to decrease in the same way.

Table 5. The pressure values at each flow characteristic measurement point in the pipe containing the DF.

		P (kPa)									
V_{inlet}		Point 1	Point 2	Point 3	Point 4	Point 5	Point 6	Point 7	Point 8	Point 9	Point 10
1.5 m/s	Line 1			8.0278	8.0941	8.1993	1.1769	1.0813	1.109		
	Line 2		8.0278	8.0315	8.0977	8.1958	1.7097	1.0801	1.0683	0.3801	
	Line 3	7.986	8.014	8.044	8.1011	8.203	5.255	1.0799	1.0594	0.3826	0.0227
	Line 4	7.9839	8.0061	8.0475	8.1034	8.215	8.2079	1.0802	1.0561	0.4198	-0.0228
	Line 5	7.9842	8.0059	8.0485	8.1033	8.2225	8.7235	1.081	1.0697	0.5462	0.0431
2 m/s	Line 1			11.1955	11.3682	11.593	2.0497	1.8764	1.9262		
	Line 2		11.2001	11.1925	11.3671	11.5954	2.7553	1.8729	1.8538	0.625	
	Line 3	11.0707	11.1533	11.2309	11.374	11.6014	7.6196	1.8715	1.8329	0.6196	0.0101
	Line 4	11.0654	11.1386	11.2425	11.3858	11.6082	11.7556	1.8725	1.8231	0.7543	-0.0024
	Line 5	11.0636	11.1408	11.245	11.3897	11.6116	12.7695	1.874	1.8293	0.8535	0.0366
2.5 m/s	Line 1			14.8	15	15.4	3.21	2.94	3.01		
	Line 2		14.5	14.8	15	15.4	4.08	2.93	2.9	0.981	
	Line 3	14.4	14.5	14.8	15	15.4	10.3	2.93	2.87	0.975	0.0182
	Line 4	14.4	14.5	14.8	15	15.3	15.5	2.93	2.85	1.18	0.0058
	Line 5	14.4	14.6	14.8	15	15.3	16.7	2.93	2.86	1.34	0.0623

It is understood that the average velocity per area increases as the pressure drop increases, according to the Darcy's law, which is generally applied to calculations in porous media. Darcy's law is expressed as Equation (6), where u_D is the average velocity per area of the fluid, Q is the flow rate, A is the cross-sectional area, K is the permeation coefficient, μ is the viscosity coefficient, and P is the pressure [19].

$$u_D = \frac{Q}{A} = -\frac{K}{\mu}\frac{\Delta P}{\Delta x} \tag{6}$$

Also, in Figure 11, the pressure in the porous zone increases toward the center of the pipe. This is because the flow per unit area near the center increases as the flow in the pipe approaches the maximum flow rate toward the center due to the no-slip condition. The resistance the working fluid receives from the viscous resistance of the filter increases in proportion to the flow rate.

4. Conclusions

In this study, a numerical analysis method was used to compare and analyze the flow characteristics and differential pressure performance of the CTCS to which a 14-inch DF was applied. As a result, the following conclusions were reached.

(1) The numerical analysis confirmed that the main flow in the pipe with the DF was dominantly affected by the vortex generated by the DF bracket.

(2) As the flow velocity increases, the radius of the vortex generated by the flow colliding with the DF bracket increases. And as the vortex radius increases, friction with the main flow is induced, leading to an increase in the TKE, which interferes with the main flow and is thought to cause flow loss in the tube.

(3) According to the Bernoulli's law, the pressure before and after the DF tends to be inversely proportional to the flow rate and pressure. On the other hand, the speed and pressure in the filter tend to be proportional, which was confirmed by calculations made using the Darcy's law on the influence of the porous zone of the perforated plate.

(4) In addition, it was confirmed that the filter shape and fluid resistance due to pressure drop in the porous zone had a dominant influence on the differential pressure performance in the pipe with the DF.

Funding: - This work was supported by the Technology Innovation Program (20018176, Development of heat exchanger cleaning system and automatic operation technology that can reduce energy use of heat exchangers by more than 25%) funded By the Ministry of Trade, Industry & Energy(MOTIE, Korea).

References

1. H. M. Chae, J. T. Kwon, D. A. Cha and O. K. Kwon, “The Measurements of Ball Recovery Rate for the Cleaning Apparatus in Plate Heat Exchanger Using Ceramic Ball”, Journal of the Korean Society for Power System Engineering, 2014, Vol. 18, No. 1, pp. 38~44
2. K. M. Nam and S. J. Kang, “A Comparative Study on Technical Efficiency in the Secondary Energy Industry and a Factor Analysis for Technical Efficiency”, Korean Energy Economic Review, 2015, Vol. 14, No. 1, pp. 111~141
3. S. C. Park and I. W. Lee, “Experimental study on analysis of correlation between void fraction and drag reduction rate in air lubrication ship”, Journal of The Korean Society of Visualization, 2020, Vol. 18, pp. 11~17.
4. Ibrahim, Said MA, and Sami I. Attia. "The influence of condenser cooling seawater fouling on the thermal performance of a nuclear power plant." Annals of Nuclear Energy 76, 2015, pp. 421~430.
5. Alabrudzinski, S., Markowski, M., Trafczynski, M., and Urbaniec, K, “The influence of fouling build-up in condenser tubes on power generated by a condensing turbine”, Chemical Engineering Transactions, 2016, Vol. 52, pp. 225~1230
6. Pattanayak. L, Narayana Padhi. B and Kodamasingh. B, "Thermal performance assessment of steam surface condenser." Case Studies in Thermal Engineering, 2019, pp.100484
7. Mohammadaliha. N, Amani. M and Bahrami. M, "Thermal performance of heat and water recovery systems: Role of condensing heat exchanger material." Cleaner Engineering and Technology, 2020, Vol. 1, pp. 100024
8. Gadhamshetty, V, Nirmalakhandan. N, Myint. M and Ricketts. C, "Improving air-cooled condenser performance in combined cycle power plants." Journal of energy engineering, 2006, Vol.132 pp. 81~88.
9. C. S. Yi, and C. W. Lee, “Development on Cleaning System of Condenser for Nuclear Power Plant by Using Sponge Ball” Journal of the Korean Society of Manufacturing Process Engineers, 2015, Vol. 14(6), pp. 21~26.
10. G. C. Jeong, H. S. Lee and C. W. Lee, “Numerical analysis of ball strainer screen module blockage effects,” Journal of the Korean Society for Power System Engineering, 2015, Vol. 19, No. 1, pp. 83~89.
11. S. J. Lee, J. S. Kim and S. H. Lee, “A study on the fouling factor and formation of surface film in the power plant condenser,” Korean Journal of materials Research, 1997, Vol. 7, No. 9. pp. 750~757.
12. C. S. Lee and C. W. Lee, “Development on Cleaning System of condenser for nuclear Power Plant by Using Sponge Ball,” Journal of the Korean Society of Manufacturing Process Engineers, 2015, Vol. 14, No. 6, pp. 21~26.
13. S. Y. Kwon, D. J. Hur and J. K. Choi, “ A study of the ball dispersion prediction for increasing the effect of condenser tube cleaning system,” Journal of computational fluids engineering, 2016, 2016 Spring Conference of KSCFE, pp. 83~84.
14. S. Y. Kwon, D. J. Hur and K. S. Yun, “Study on the Prediction of Ball Collection Rate in Power Plants Condenser Tube Cleaning System,” Trans. Korean Soc. Mech. Eng. 2017, 2017 Spring Conference of KSME, pp. 61~62.
15. M. S. Jung, and K. T. Kim, "Debris filtering efficiency and its effect on long term cooling capability." Nuclear Engineering and Design, 2013, Vol. 261 pp. 1~9
16. Walker, M. E., Safari, I., Theregowda, R. B., Hsieh, M. K., Abbasian, J., Arastoopour, H., ... & Miller, D. C. “Economic impact of condenser fouling in existing thermoelectric power plants”, Energy, Vol. 44, pp. 429~437

Preprints (www.preprints.org) | NOT PEER-REVIEWED | Posted: 17 April 2023 doi:10.20944/preprints202304.0412.v1

17. Y. W. Kim, J. R. Goo, Y. C. Bae, H. Lee and Y. S. Lee, “Vibration Phenomena between Condensate Vertical Pump and Condenser Debris system in Power Plant”, 2001, Trans. Korean Soc. Noise Vib. Eng., pp. 1020~1025
18. Zubair, S. M., Sheikh, A. K., Younas, M., & Budair, M. O. “A risk based heat exchanger analysis subject to fouling: Part I: Performance evaluation”, Energy, 2000, Vol. 25, pp. 427~443.
19. S. W. Choi, J. H. Yang, B. S. Kim and J. S. Kwon, “Study on permeability coefficient and fluid behavior of porous materials”, 2018, Journal of the Korean Society of Marine Engineering, Vol. 42, No. 9 pp. 742~746